Journal of Alloys and Compounds, 207/208 (1994) 153–160
JALCOM 3008

Rare earth crystal field spectroscopy by neutron magnetic scattering: from xenotime to high T_c superconductors

C.-K. Loong and L. Soderholm
Argonne National Laboratory, Argonne, IL 60439-4814 (USA)

Abstract

Optical spectroscopy is one of the traditional methods used to determine the overall splitting of the rare earth ion energy states within an f^N configuration in either solution or solid state of transparent materials. This technique can provide data over a wide energy range with good resolution, and the parameters obtained for the empirical Hamiltonian reflect the "best fit" of the observed energies. Absolute intensity measurements of optical transitions and their comparison with theory, however, are difficult. Magnetic scattering of thermal neutrons arises from an interaction of the neutron magnetic moment with the convection and spin current of the scatterer. Such a weak interaction does not involve any excited intermediate states of the system and requires only a first-order perturbation treatment to calculate the scattering cross-section. However, neutron spectroscopy probes only states at energies less than ~1 eV. It is demonstrated that a combined treatment of neutron and optical data can provide the complementary information necessary for a proper characterization of the level splittings and wavefunctions of the rare earth ions in xenotime (RPO_4, R = Tb to Yb). Next we discuss the analyses of neutron scattering data for the understanding of the rare earth energy levels and wavefunctions in various high T_c copper oxide superconductors and related compounds. The importance of a consistent refinement of the crystal field parameters across a series of isostructural rare earth compounds and a systematic comparison of the low temperature magnetic properties with model calculations are emphasized.

1. Introduction

4f electronic transitions play an important role in the optical and magnetic behavior of rare earth bearing materials. For rare earth ions in crystalline solids, optical spectroscopy has been applied with great success in the characterization of the crystal field split 4f states as well as interactions of the 4f electrons with the local environment. In this paper, we try to point out the complementarity of using neutron magnetic scattering to study the energy splitting and wavefunctions of rare earth low-lying states, especially in stoichiometric compounds and optically opaque materials. If both optical and neutron data are available, a combined analysis provides additional self-consistency checks for the correctness of the parametric single-ion Hamiltonian. If cooperative effects such as magnetic or superconducting ordering are involved, neutron inelastic scattering may also yield useful information regarding the dynamic nature of the interactions responsible.

The subject of optical spectroscopy of f-electron systems has already been discussed extensively in a number of monographs [1,2] and review articles [3,4]. Here we only outline briefly the major differences and similarities between electronic Raman scattering (and absorption) and neutron magnetic scattering. We do not discuss rare earth activated luminescence, an equally important aspect in optical spectroscopy, because our main concern is rare earth ground state properties. Our discussion of electronic Raman effects follows closely that given previously by Downer [5]. In his work, Downer also reviewed the results and the remaining puzzles of Raman scattering studies of rare earth orthophosphates (xenotime) by Becker and co-workers [6–10], with which recent neutron scattering data of xenotime [11–14] is compared later in this paper. Electronic Raman scattering for rare earth ions involves transitions from an initial $|4f^N,m\rangle$ to a final $|4f^N,n\rangle$ state via excited intermediate states $|4f^{N\pm1},\beta\rangle$, of which the scattering amplitude is calculated by second- (or higher-) order perturbation theory. Odd parity, static or vibronic components of the crystal field terms which mix states from an opposite parity intermediate configuration into the $4f^N$ wavefunctions, was first proposed by van Vleck to explain the forbidden electric-dipole, one-photon transitions [15]. This phenomenon was later developed into a quantitative theory by Judd [16] and Ofelt [17]. The theory introduced a closure relation to perform a piecewise summation over subgroups of non-interacting intermediate states as an approximation to

SSDI 0925-8388(93)03008-7

the otherwise intractable sum in the second-order expansion. Intermediate states of configuration $4f^{N-1}5d$ are usually assumed to be more important than other configurations such as $4f^{N-1}ng$ and d^94f^{N+1}.

The Judd–Ofelt method was first extended to two-photon transitions by Axe [18] and subsequently treated by other workers [19–22]. Under the Judd–Ofelt approximation in a second-order expansion, the two-photon absorption strength does not involve a sum of reduced matrix elements each associated with phenomenological prefactors such as the Judd–Ofelt parameters in one-photon processes. Consequently, the observed intensity ratio of two absorption lines can be compared readily with the ratio of the squares of the corresponding second-rank reduced matrix elements given by the theory. Furthermore, in two-photon Raman scattering, the first- and second-order terms arise from the antisymmetric and symmetric contributions to the scattering tensor $\alpha_{\rho\sigma}$, respectively. ($\alpha_{\rho\sigma}$ is symmetric if $\alpha_{\rho\sigma}=\alpha_{\sigma\rho}$ and asymmetric if $\alpha_{\rho\sigma}=-\alpha_{\sigma\rho}$, where ρ and σ denote the polarizations of the incident and scattered photons, respectively.) A measurement of the sign and magnitude of asymmetry, in terms of the symmetry ratio F_1/F_2 defined by Koningstein and Mortensen [23], provides an estimate of the relative importance of intermediate states of $4f^{N-1}5d$ and $4f^{N-1}ng$ character. Experimental determination of the absolute intensities for two-photon processes is difficult, only order-of-magnitude comparison with theory has been achieved so far [24,25]. Analyses of two-photon spectra usually rely on a comparison of relative intensities of different transitions.

The strong photon–atom interaction also gives rise to other processes such as various electric and magnetic multipolar transitions, hypersensitive transitions in one-photon transitions, resonance-enhanced scattering, third- and fourth-order contributions to two-photon transitions, as well as secondary processes which involve radiative (luminescence) and non-radiative energy transfers [1–5,26,27]. Therefore, analyses of experimental data have to be done carefully. Critical review of rare earth optical data to quantitatively differentiate the various one- and two-photon processes has not been done, except for the lanthanide doped fluoride [5,28] and phosphate [6–10] systems.

The magnetic scattering of thermal neutrons arises from an interaction of the neutron magnetic moment (-1.91 nuclear magneton) with the convection and spin current of the scatterer. Such a weak interaction does not involve any excited intermediate states of the system and requires only a first-order perturbation treatment (the Born approximation). For a system of non-interacting ions with f^N configurations, the convection and spin current operator is related to the total (orbital and spin) angular momentum operator of N equivalent f-electrons, which can be expanded in multipole fields using spherical tensor techniques [29]. For thermal neutron scattering at small wavevectors, as is the usual case, only magnetic dipole transitions need to be considered. This simplicity of the neutron scattering process permits a quantitative comparison to be made of the observed absolute intensity and the crystal field model calculation in a straightforward manner.

Neutron magnetic scattering usually probes only the low-lying states within the Russell–Saunders ground multiplet of a rare earth ion [30]. Optical spectroscopy, on the other hand, is optimized for measurements of high energy levels with good resolution. A combined treatment of neutron and optical data thus provides complementary information necessary to a complete characterization of the energy splitting of a f^N configuration. In addition, since the wavelength of thermal neutrons (≈ 1 Å) is comparable to the atomic distances in solids, the momentum transfer dependence of the neutron magnetic and nuclear scattering spectra are related to spatial correlations of the magnetic excitations (*e.g.* magnons) and atomic vibrations (*e.g.* phonons), respectively, through Fourier transforms. The photon wavelengths of the infrared to ultraviolet region are much larger than the dimension of the unit cell of crystalline solids, so optical spectroscopy measures electronic excitations and phonons only at the Brillouin zone center. If collective excitations are involved (*e.g.* spin waves, electron-phonon coupling), neutron scattering provides useful information to complement analysis of mode-coupling or energy transfer effects (*e.g.* phonon and magnon sidebands, vibronic excitations) in optical data.

In addition to the weak neutron atom scattering, severe nuclear absorption of neutrons does not occur except for a handful of isotopes. (For rare earth compounds containing samarium, europium and gadolinium, neutron scattering experiments can only be performed using samples with the rare earth elements replaced by non-absorbing isotopes.) Therefore, neutrons probe the bulk of most materials and are usually not sensitive to minute impurities and surface effects. Optical absorption studies, on the other hand, are restricted to optically transparent materials or rare earths doped into optically inactive host solids. Light sources such as lasers provide bright, monochromatic beams sufficient for studying small samples (<1 g) whereas available fluxes from neutron sources are relatively low and large samples (10–100 g) are needed. In principle, neutron spin polarization analysis can be applied to single crystal experiments for a detailed characterization of the scattering processes. However, for basic studies of rare earth crystal field level structure, polycrystalline samples and unpolarized neutron experiments are often adequate.

Combined analyses of both neutron and optical data for rare earth energy levels are rare in the literature. We present examples from recent studies of rare earth orthophosphates (xenotime) and high T_c superconductors. Experimental details concerning the neutron scattering experiments have been given previously elsewhere [11,12].

2. Xenotime (RPO_4, R=Tb to Lu)

Mixed natural rare earth orthophosphates, RPO_4, form the minerals monazite (R=La to Gd, crystal structure: monoclinic, space group $P2_1/n$) and xenotime (R=Tb to Lu, tetragonal, $I4_1/amd$). Pure crystalline forms of these compounds can be synthesized by controlled precipitation techniques [31], and single crystals can be grown by means of flux methods [32]. The optical and magnetic properties of rare earth ions in RPO_4 hosts, including their rare earth activated luminescence, magnetic phase transition, and Jahn–Teller effects, have been the focus of numerous experimental and theoretical investigations [33]. Some basic properties of these materials are illustrated in Fig. 1. Recently, Becker and co-workers [6–10] have performed both non-resonance and resonance electronic Raman scattering on single crystals of stoichiometric $HoPO_4$, $ErPO_4$, $TmPO_4$, and $YbPO_4$. Detailed comparisons of the observed and predicted relative Raman line intensities and polarization anisotropies were made. Although the analyses have led to the assignments of a large portion of the crystal field split states in many multiplets of energies up to 30 000 cm^{-1}, there remained a number of outstanding discrepancies between the theory and experiments which, along with other similar contradictions in other systems, prompted concern for the "new puzzle of two-photon rare earth spectra in solids" raised by Downer [5] (as opposed to the old puzzle of one-photon electric dipole-transitions that was put forward by van Vleck [15] in 1937).

Our neutron scattering studies of xenotime were motivated by several considerations. First, the neutron data supplement the optical data that are incomplete at low energies thereby allowing a better characterization of the ground state. Second, neutron scattering provides a measure of the phonon densities-of-states and an estimate of cooperative effects such as spin-spin and spin-lattice coupling, if any, at low temperatures. Third, systematic analyses of neutron and optical data are helpful in assessing the extent to which the rare earth free-ion parameters can vary among different host materials. In particular, it is of interest to determine the effects, if any, that result from the adoption of the lanthanide trifluoride free-ion parameters in the analysis of the neutron crystal field spectra of the rare earth

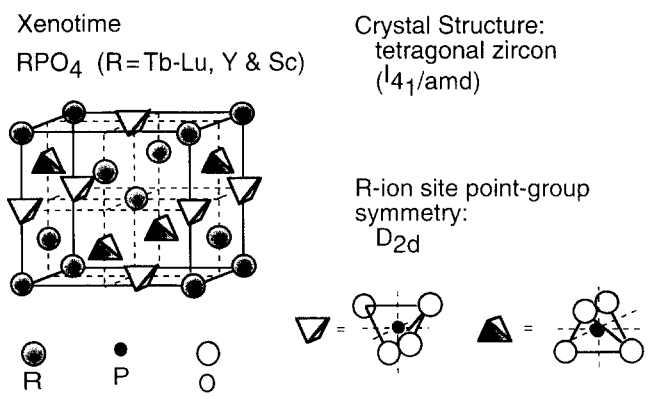

RPO_4: R	Tb	Dy	Ho	Er	Tm	Yb
T_N (K)	2.2	3.4	1.35	<0.4		
Ground state (major J,J_M)	$6,\pm5$	$\frac{15}{2},\pm\frac{15}{2}$	$8,\pm7$	$\frac{15}{2},\pm\frac{7}{2}$	6,0	$\frac{7}{2},\pm\frac{3}{2}$
$g_{//}$	12.7	19.4	17.2	6.6	0	1.6
$g_{\perp}$	0	~0	0	4.3	0	3.2
Estimated exchange field (kG)	5.2	3	2.4			

Fig. 1. Upper diagram: the unit cell of xenotime, which contains four formula units of RPO_4. Lower portion: the Néel temperatures, J_M of the major components $|J,J_M\rangle$ in the ground state wavefunctions, spectroscopic splitting g-factors of the ground states ($\|$ and $\perp$ denote the magnetic field directions parallel and perpendicular to the c-axis, respectively), and the exchange field strength estimated from a molecular-field approximation.

copper oxide superconductors [34]. We discuss the neutron results by presenting examples of the $TmPO_4$, $ErPO_4$ and $HoPO_4$ data and analyses.

The observed and calculated neutron scattering spectra for $TmPO_4$ at 15 and 100 K are shown in Fig. 2. The observed position of a crystal field peak is equal to the energy separation of the two crystal field states (*e.g.* $|4f^N,i\rangle$ and $|4f^N,j\rangle$) that participate in the transition, and the intensity is proportional to the square of the matrix element $\langle 4f^N,i|J_\perp|4f^N,j\rangle$ (where $J_\perp$ is the component of the total angular-momentum operator perpendicular to the neutron wavevector). The calculated spectra were obtained by fitting the data to the same crystal field model used by Becker and co-workers [6–10], namely, a single-ion model based on the scheme of intermediate coupling using the spherical tensor formalism [35–37]. Because of the simplicity of neutron magnetic scattering by non-interacting ions, the scattering function, $S(E)$, can be calculated in a straightforward manner [11,12]. Since both the energies and intensities at all temperatures were used in the fits, all five parameters, B_0^2, B_0^4, B_4^4, B_0^6 and B_4^6, needed in order to characterize the crystal field potential can be

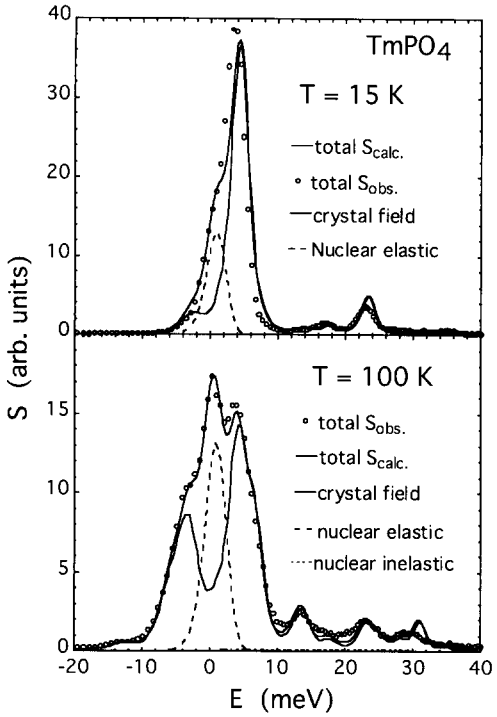

Fig. 2. The observed (symbols) and calculated (curves) neutron scattering functions for $TmPO_4$.

obtained unambiguously. The analysis benefited from the knowledge of the Tm^{3+} free-ion parameters (which were fixed throughout the analysis) and the symmetry assignment of the states obtained previously from the optical studies by Becker *et al.* Details concerning the crystal field model, neutron scattering cross-section, the relation between the observed transition strength and the spectroscopic splitting g-factors have been given elsewhere [11,12,35–37].

One of the most significant findings from electronic Raman scattering of $TmPO_4$ was that the observed asymmetries of the low energy Γ_5 and Γ_3 lines can only be fitted by symmetry ratios of $F_1/F_2 = 0.25$ and -0.03, respectively [6,7,10]. These small ratios would indicate approximately equal contributions of the $4f^{N-1}ng$ and $4f^{N-1}5d$ configurations to the two-photon processes. However, the very strong calculated relative intensities of two crystal field lines (Γ_1 and Γ_4) near 250 cm^{-1} for various polarization anisotropies, assuming either a dominant $4f^{N-1}ng$ or equal $4f^{N-1}ng$ and $4f^{N-1}5d$ configurations, were contradicted by the non-observable intensities. Smentek-Mielczarek [38] extended the calculations of the Raman intensities and polarization characteristics to include contributions from the third-order perturbed functions but found only relatively small improvements. Xia [39] proposed a decay mechanism involving two E_g^1-type phonons to explain the absence of the ground-state-to-Γ_1 and -Γ_4 transitions in the Raman spectrum. Our results clearly showed that the positions and intensities of the Γ_1 and Γ_4 states are in agreement with the crystal field model (see Fig. 2). In addition to the four states previously identified by Raman scattering [6–8], we observed five transitions to the Γ_1 (30.5 meV), Γ_4 (34.5 meV), and the closely spaced Γ_3 and Γ_4 (42 meV) states thereby establishing the positions of these states [11]. No phonon anomalies were found in $TmPO_4$ within the experimental uncertainty of the neutron experiments using polycrystalline samples. Similar inconsistencies in the observed and calculated asymmetries and relative intensities for the Raman data can also be seen in the cases [5–7] of $HoPO_4$ and $ErPO_4$. Therefore, the discrepancies in the Raman scattering studies appear to be caused by the complexity of the intermediate states participating in the Raman scattering and not some inherent problem of the ground state.

The typical, observed and calculated neutron spectra for $HoPO_4$ and $ErPO_4$ are displayed in Fig. 3. In the case of $HoPO_4$, the combined analysis of the neutron [12] and optical data obtained previously by Enderle *et al.* [40] permits a satisfactory refinement of the three Slater–Condon electrostatic parameters for the free-ion part of the Hamiltonian and the five crystal field parameters. The excellent agreement between the calculated energies and the observed neutron and optical energies is represented by an overall root-mean-square (rms) energy deviation of 3.2 cm^{-1} for all the Ho ^5I multiplets extended the about 11 000 cm^{-1}. The calculated energies for the $^3K_7$ and the $^3H_6$ states, on the other hand, differ systematically from those measured by Enderle *et al.* [40] (with a rms deviation greater than 100 cm^{-1}). These disagreements involving the high energy states are attributed to effects of electronic correlation on the crystal field that are not considered in the one-electron crystal field Hamiltonian. Pilawa and co-workers [41] have recently investigated this problem and achieved significant improvements in the fits to data ranging from 0 to 28 000 cm^{-1} for Ho^{3+} in the hosts of YVO_4, $YAsO_4$, and $HoPO_4$ by introducing additional (L,S)-term-dependent crystal field parameters [42].

For $ErPO_4$, it is of interest to compare the neutron data [12] with the optical results because all the ground multiplet states of Er^{3+} in $ErPO_4$ have previously been identified by non-resonance and resonance-enhanced electronic Raman scattering by Becker *et al.* [7]. Significant enhancement of the two-photon scattering amplitude was achieved by using the argon ion laser excitation line at 488.0 nm that coincides with the Er^{3+} $^4I_{15/2} \rightarrow {}^4F_{7/2}$ transition in $ErPO_4$. In general, we found good agreement between the neutron and Raman data except for two energy levels, *i.e.* the third Γ_7 state (neutron 17.1 meV; Raman 13.0 meV) and the highest Γ_6 state (neutron 40 meV; Raman 33.4 meV) (1 meV is equivalent to 8.066 cm^{-1}). The intensities for exci-

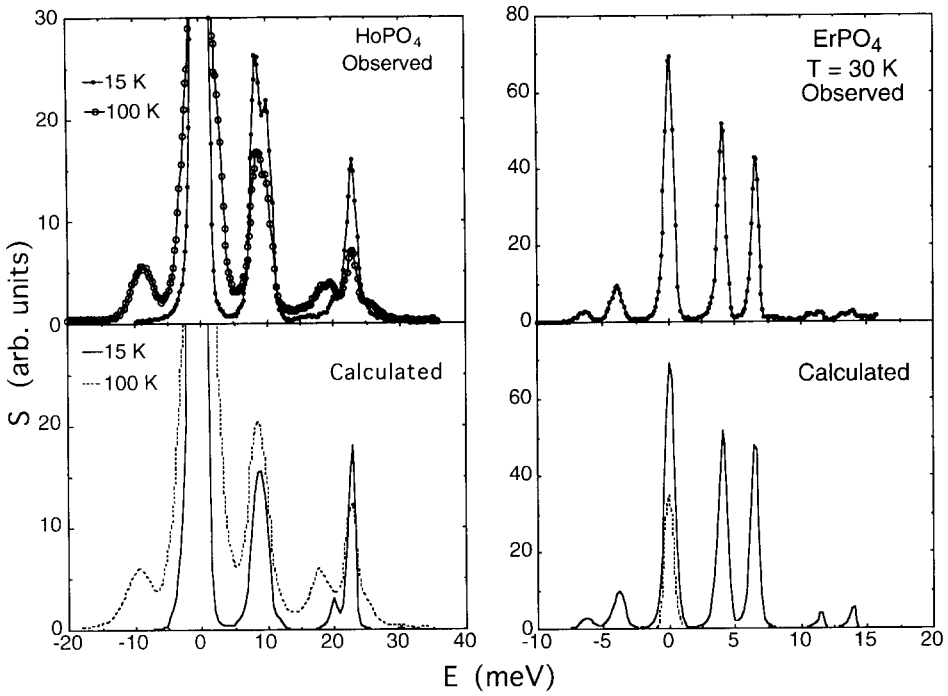

Fig. 3. The observed (upper panels) and calculated (lower panels) neutron scattering functions for $HoPO_4$ and $ErPO_4$. The lines in the observed spectra are guides to the eye. The solid line in the calculated spectrum of $ErPO_4$ represents the sum of magnetic- and nuclear elastic (dashed line) scattering.

tations from the ground states to these two levels are weak in both the neutron and Raman experiments. At present, the reason for the discrepancies in the energies of these two levels observed in the neutron and optical studies is not yet known.

The rare earth low-lying crystal field states determine the nature of the magnetocrystalline anisotropy and the details of magnetic interactions with other ions at low temperatures. We find that the rare earth crystal field level structure derived from the neutron scattering studies provide a basis for explaining the low temperature magnetic properties of RPO_4. For example, the calculated paramagnetic susceptibilities for xenotime agree well with data obtained from single crystal measurements. The antiferromagnetic ordering of the rare earth moments in $TbPO_4$, $DyPO_4$ and $HoPO_4$ can be understood by the highly anisotropic magnetization along the crystallographic c-axis of the rare earth ground states, which favor spin-coupling along the easy axis (c-axis). On the other hand, the lack of magnetic ordering for $ErPO_4$, $TmPO_4$ and $YbPO_4$ can be explained by the rather isotropic magnetization density of the Er^{3+} and Yb^{3+} ground states, and the non-magnetic singlet ground state in $TmPO_4$. Other results [11–14] derived from neutron scattering studies regarding the rare earth crystal field ground state wavefunctions, spectroscopic splitting g-factors and estimated exchange field strengths (for the magnetically ordered members) for the RPO_4 system are summarized in Fig. 1.

3. High T_c rare earth copper oxide superconductors

Co-existence of rare earth magnetism and superconductivity has been found in the $RBa_2Cu_3O_7$ (R = rare earths except for Pr), $R_{2-x}M_xCuO_4$ (R = Pr, Nd and Sm; M = Ce or Th; $0.14 < x < 0.18$), $RBa_2Cu_4O_8$ (R = Nd to Er except for Tb), and $Pb_2Sr_2R_{0.5}Ca_{0.5}Cu_3O_8$ (R = Pr to Lu) systems [43]. Neither the paramagnetic or the antiferromagnetically ordered moments of the rare earth ions appear to interact with the charge carriers in the CuO sublattice. Our interest in the crystal field level structure of the rare earth ions in these materials has been focused on the selectively adverse effects of some rare earth elements on superconductivity, in particular, the interplay between spin dynamics of the Pr ions and suppression of superconductivity in $Y_{1-x}Pr_xBa_2Cu_3O_7$.

Although the usefulness of rare earth crystal field excitations as a probe of the local electronic symmetry and possible interactions with the superconducting charge carriers (in the CuO planes) has been long recognized, the determination of the level structure of rare earth ions in high T_c superconductors by neutron spectroscopy has been difficult. First, the rather low point-group symmetry of the rare earth sites requires a significant number of parameters for the description of the crystal field potential (9 for an $RBa_2Cu_3O_7$ compound). Second, optical absorption measurements cannot be used because these materials are optically opaque, and Raman studies are complicated because

the spectra contain many non-crystal field features. Inelastic neutron scattering reveals only a handful of crystal field transitions for a typical compound (*e.g.* four peaks for $NaBa_2Cu_3O_7$). Third, the large (≈ 100 meV) splitting of the ground multiplet may result in significant mixing of some higher J-multiplet states into the low-lying states, especially for the light rare earth compounds, so a crystal field model formulated under the scheme of intermediate coupling is necessary.

The first successful refinement of neutron data for determining the crystal field parameters was achieved by Furrer *et al.* [44] on $HoBa_2Cu_3O_7$. Since the next higher J-multiplet of Ho^{3+} is far away from the ground multiplet, these authors used the Steven's operator equivalents method [45] to first assess the important parameters based on an approximate cubic symmetry for the rare earth sites. Other crystal field parameters were then added to expand the analysis to the appropriate orthorhombic symmetry until a self-consistent refinement was accomplished. To circumvent the paucity of well-defined transitions for each material, we worked towards a systematic analysis of the crystal field spectra for several isostructural compounds to look for a reasonable correlation among the corresponding crystal field parameters for the rare earth ions and an overall consistency between the model predictions and observed data. We used an intermediate-coupling crystal field model [35–37] of which the rare earth free-ion parameters established previously [37] for $R:LaF_3$ were adopted and fixed in the model calculation. These free-ion parameters are expected to be insensitive to the different crystal structures of the hosts. The crystal field parameters for $HoBa_2Cu_3O_7$ obtained by Furrer *et al.* [44] were first converted to be used in the intermediate-coupling, spherical tensor formulated model [34] and the spectra were re-analyzed to ensure a consistency with the operator equivalents method [34]. The parameters were then scaled to the corresponding values for $NdBa_2Cu_3O_7$ and $PrBa_2Cu_3O_7$ according to the radial integral, $\langle r^n \rangle$, of the 4f radial wavefunctions. Using the scaled parameters as initial values for the fits of the neutron data, the refinements yielded satisfactory results. This method has been thoroughly tested [46–48] also for Er, Dy, Eu and Sm compounds of the $RBa_2Cu_3O_7$ series, and for other systems [49,50]. In some cases, additional information was also obtained, such as using the superposition model [51] to transfer the intrinsic crystal field parameters from one system to another or estimating the second-order parameters from Mössbauer data [46–49], to aid the analyses. The satisfactory description of the paramagnetic susceptibilities and specific heats by the crystal field calculation for many of these materials [34,46–50] further lends credence to the applicability of this method.

Good agreement between the observed and calculated scattering functions for superconducting $NdBa_2Cu_3O_7$ can be seen in Fig. 4. The calculated magnetic susceptibility agrees well with the experimental data [34]. The sharp peaks of $NdBa_2Cu_3O_7$ at 15 K indicate that the lifetimes of the single ion crystal field excitations are relatively long and there is little interaction of the Nd^{3+} 4f-states with the environment. However, the rather low resolution neutron scattering measurements using polycrystalline samples did not provide enough details to permit an analysis of the more subtle features. Recent Raman studies [52] using $NdBa_2Cu_3{}^{16}O_7$ and $NdBa_2Cu_3{}^{18}O_7$ single crystals with polarization analysis have revealed evidence of coupling of crystal field excitations to phonons at energies near 37.5 meV in $NdBa_2Cu_3O_7$. The effect of an applied magnetic field on the coupled crystal field-phonon states was also investigated [53] and the results were analyzed in terms of Zeeman splitting of the crystal field state wavefunctions obtained previously from neutron measurements [34,54]. This series of neutron and Raman scattering measurements have demonstrated very well the complementarity of the two techniques in the study of rare earth electronic structure.

The background corrected, observed and calculated scattering functions for insulating $PrBa_2Cu_3O_7$ are shown in Fig. 5. The magnetic excitation spectrum of $PrBa_2Cu_3O_7$ in general agrees with the crystal field calculation for an f^2 configuration, thus supporting a predominantly trivalent state of the Pr ions [34]. How-

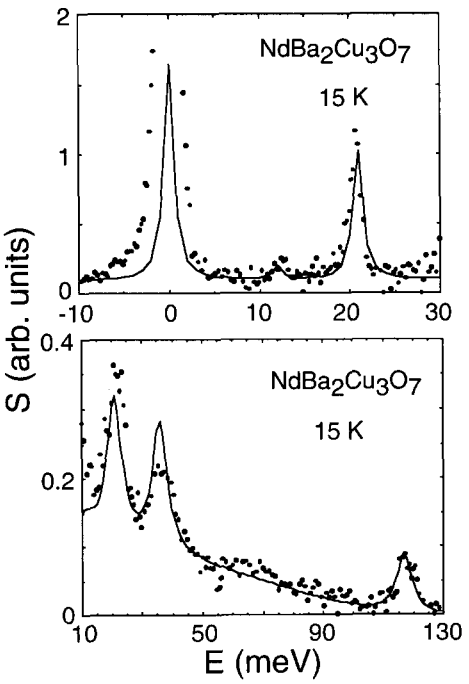

Fig. 4. The observed (symbols) and calculated (curves) neutron scattering functions for $NdBa_2Cu_3O_7$.

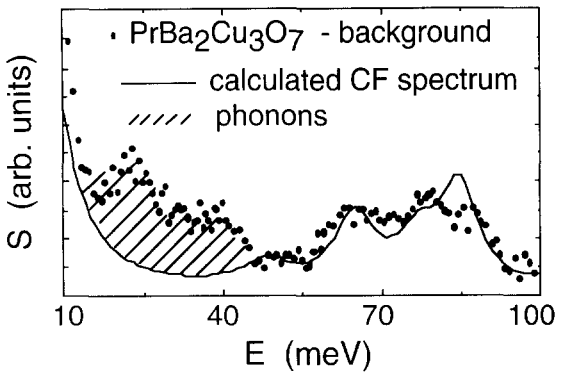

Fig. 5. The background-corrected, observed total scattering (symbols) and calculated magnetic scattering (solid line) for $PrBa_2Cu_3O_7$. The shaded area represents non-magnetic phonon scattering.

ever, the intrinsic linewidths for the crystal field peaks (about 3.9 and 9 meV for the excitations below and above 20 meV, respectively) are significantly larger than those of magnetic superconductors such as $NdBa_2Cu_3O_7$ and $ErBa_2Cu_3O_7$ [46]. Since superconductivity is suppressed entirely in $Y_{1-x}Pr_xBa_2Cu_3O_7$ for $x > 0.4$, the neutron results suggest that strong fluctuations of the Pr spins within the low-lying crystal field levels couple to CuO electron-hole excitations may significantly affect the transport properties of the materials, including superconductivity. In order to test this premise further, we measured the magnetic excitation spectra of two other reference non-superconducting compounds, $PrScO_3$ and Pr_2CuO_4 [34,49]. Both compounds clearly show sharp, well-defined crystal field excitations. In $PrScO_3$ the Pr^{3+} ions experience a similar distorted perovskite crystal field environment, but unlike $Y_{1-x}Pr_xBa_2Cu_3O_7$, there are no conduction electrons available for coupling to the Pr f-electrons in $PrScO_3$. In Pr_2CuO_4, superconductivity does not occur unless Pr is partially substituted by Ce. Both $PrBa_2Cu_3O_7$ and Pr_2CuO_4 have a non-magnetic ground state but the first excited state of Pr^{3+} ions in Pr_2CuO_4 is located at 18 meV (209 K) whereas in $PrBa_2Cu_3O_7$ there are three almost degenerate excited states below 4 meV (46 K). Therefore, the cumulative evidence suggests two characteristics of the Pr ions which together may play a crucial role in suppressing superconductivity: (1) the spatially extended f-orbital of Pr ions favors magnetic interaction or hybridization between the f- and the CuO-electrons; (2) the availability of low-lying crystal field states permits the unpaired electrons to undergo spin-flip transitions with minimal energy cost, thereby creating unfavorable conditions for electron (or hole) pairing at low temperatures.

4. Conclusions

We briefly discussed the similarities and differences in the techniques of electronic Raman and magnetic neutron scattering for studies of rare earth energy level structure. Optical absorption (for optically transparent materials) and Raman scattering allow measurements of f-states over a wide range of energies with good resolution. Optical experiments can be performed on small single crystals. The incident and scattered photon polarization and asymmetry ratios of transition strength can be analyzed to provide additional information regarding the nature of the scattering/absorption processes and the excited intermediate states involved. However, measurements of absolute intensities are difficult experimentally, and Judd–Ofelt-like approximations have to be applied to calculate the scattering amplitude theoretically. Serious disagreements between the observed and predicted two-photon spectra remain in many systems. Neutron scattering studies, on the other hand, are ideal for studying the low-lying f-states and cooperative interactions in most bulk materials. However, the paucity of observed transitions together with the relatively poor signal-to-noise ratios of neutron measurements often hamper the determination of crystal field parameters and the detailed, quantitative analysis of some weak features. A combined treatment of optical and neutron data across a series of rare earth isostructural compounds, if available, often provides the complementary information needed for a full characterization of the rare earth energy level structure as well as magnetic interactions with the environment. We showed examples of such analyses in xenotime and high T_c superconductors. In both cases the crystal field parameters were obtained and the analyses led to better understanding of many important effects of rare earth magnetism on the optical and transport properties of these materials.

Acknowledgment

We are indebted to the many collaborators: M.M. Abraham, L.A. Boatner, B.D. Dabrowski, N. Edelstein, G.L. Goodman, J.P. Hammonds, and S. Kern with whom we have enjoyed working in the course of these studies. Work performed at Argonne National Laboratory is supported by the U.S. DOE, Basic Energy Sciences under Contract Nos. W-31-109-ENG-38.

References

1 G.H. Dieke, *Spectroscopic Properties of Rare Earth Ions in Crystals*, Wiley, New York, 1968.

2 S.H. Hüfner, *Optical Spectra of Transparent Rare Earths Compounds*, Academic Press, New York, 1978.
3 A.A. Kaplyanskii and R.M. MacFarlane (eds.), *Spectroscopy of Solids Containing Rare Earth Ions*, North-Holland, Amsterdam, 1987.
4 B.R. Judd, in K.A. Gschneidner, Jr. and L. Eyring (eds.), *Handbook on the Physics and Chemistry of Rare Earths*, Vol. 11, North-Holland, Amsterdam 1988, p. 81.
5 M.C. Downer, in W.M. Yen (ed.), *Laser Spectroscopy of Solid II*, Springer-Verlag, Berlin 1989, p. 28.
6 P.C. Becker, Electronic Raman scattering in rare earth phosphate crystals, Ph. D. Thesis, Lawrence Berkeley Laboratory, University of California, Berkeley, 1986.
7 P.C. Becker, N. Edelstein, G.M. Williams, J.J. Bucher, R.E. Russo, J.A. Koningstein, L.A. Boatner and M.M. Abraham, *Phys. Rev. B, 31* (1985) 8102; P.C. Becker, G.M. Williams, R.E. Russo, N. Edelstein, J.A. Koningstein, L.A. Boatner and M.M. Abraham, *Opt. Lett., 11* (1986) 282.
8 S. Guha, *Phys. Rev. B, 23* (1981) 6790.
9 P.C. Becker, N. Edelstein, B.R. Judd, R.C. Leavitt and G.M.S. Lister, *J. Phys. C, 18* (1985) L1063; G.M. Williams, P.C. Becker, N. Edelstein, L.A. Boatner and M.M. Abraham, *Phys. Rev. B, 40* (1989) 1288.
10 P.C. Becker, G.M. Williams, N. Edelstein, J.A. Koningstein, L.A. Boatner and M.M. Abraham, *Phys. Rev. B, 45* (1992) 5027.
11 C.-K. Loong, L. Soderholm, M.M. Abraham, L.A. Boatner and N.M. Edelstein, *J. Chem. Phys., 98* (1993) 4214.
12 C.-K. Loong, L. Soderholm, J.P. Hammonds, M.M. Abraham, L.A. Boatner and N.M. Edelstein, *J. Phys.: Condensed Matter, 5* (1993) 5121; *J. Appl. Phys., 73* (1993) 6069.
13 C.-K. Loong, L. Soderholm, G.L. Goodman, M.M. Abraham and L.A. Boatner, *Phys. Rev. B, 48* (1993) 6124.
14 C.-K. Loong, L. Soderholm, J.S. Xue, M.M. Abraham and L.A. Boatner, *J. Alloys Comp., 207/208* (1994) 165.
15 J.H. van Vleck, *J. Phys. Chem., 41* (1937) 67.
16 B.R. Judd, *Phys. Rev., 127* (1962) 750.
17 G.S. Ofelt, *J. Chem. Phys., 37* (1962) 511.
18 J.D. Axe, Jr., *Phys. Rev., 136* (1964) A42.
19 J.A. Koningstein and O.S. Mortensen, in A. Anderson (ed.), *The Raman Effect*, Vol. 2, Marcel Dekker, New York, 1973, p. 519.
20 H. Mahr, in H. Rabin and C.L. Tang (eds.), *Quantum Electronics: Nonlinear Optics*, Vol. 1, Academic Press, New York, 1975, p. 287.
21 R.J.H. Clark and T.J. Dines, in R.J.H. Clark and R.E. Hester (eds.), *Advances in Infrared and Raman Spectroscopy*, Vol. 9, Heyden, London, 1982, p. 282.
22 M.C. Downer, Two-photon spectroscopy of rare earth ions in condensed matter environments, Ph. D. Thesis, Harvard University, 1983.
23 J.A. Koningstein and O.S. Mortensen, *Phys. Rev., 168* (1968) 75.
24 J.P. Hermann and J. Ducuing, *Phys. Rev. B, 5* (1972) 2557.
25 L.L. Chase and S.A. Payne, *Phys. Rev. B, 34* (1986) 8883.
26 R.D. Peacock, *Structure Bonding, 22* (1975) 83.
27 R. Reisfeld, *Structure Bonding, 30* (1976) 65.
28 M.C. Downer, A. Bivas and N. Bloembergen, *Opt. Commun., 41* (1982) 335; M.C. Downer and A. Bivas, *Phys. Rev. B, 28* (1983) 3677; M.C. Downer, C.D. Cordero-Montalvo and H. Crosswhite, *Phys. Rev. B, 28* (1983) 4931.
29 C. Stassis and H.W. Deckman, *J. Phys. C, 9* (1976) 2241.
30 The recent advent of spallation neutron sources has extended the neutron scattering capability to measurements of rare earth intermultiplet transitions although the energy range is still very limited as compared to optical spectroscopy; see: R. Osborn, E. Balcar, S.W. Lovesey and A. D. Taylor, in K.A. Gschneidner, Jr. and L. Eyring (eds.), *Handbook on the Physics and Chemistry of Rare Earths*, Vol. 14, North-Holland, Amsterdam, 1992.
31 M.M. Abraham, L.A. Boatner, T.C. Quinby, D.K. Thomas and M. Rappaz, *Radioactive Waste Management, 1* (1980) 181.
32 R.S. Feigelson, *J. Am. Ceram. Soc., 47* (1964) 257.
33 See references cited in Refs. 11–14.
34 L. Soderholm, C.-K. Loong, G.L. Goodman and B.D. Dabrowski, *Phys. Rev. B, 43* (1991) 7923; G.L. Goodman, C.-K. Loong and L. Soderholm, *J. Phys.: Condensed Matter, 3* (1991)49.
35 B.G. Wybourne, *Spectroscopic Properties of Rare Earths*, Wiley, New York, 1965.
36 H.M. Crosswhite and H. Crosswhite, *J. Opt. Soc. Am. B, 1* (1984) 246.
37 W.T. Carnall, G.L. Goodman, K. Rajnak and R.S. Rana, *J. Chem. Phys., 90* (1989) 3443.
38 L. Smentek-Mielczarek, *J. Chem. Phys., 94* (1991) 5369.
39 S. Xia, *Int. J. Mod. Phys. B, 6* (1992) 59.
40 M. Enderle, B. Pilawa and H.G. Kahle, *J. Phys.: Condensed Matter, 2* (1990) 4711.
41 B. Pilawa, *J. Phys.: Condensed Matter, 3* (1991) 655, 667 and 4293.
42 B.R. Judd, *Phys. Rev. Lett., 39* (1977) 242; H. Crosswhite and D. J. Newman, *J. Chem. Phys., 81* (1984) 4959; Y.Y. Yeung and D.J. Newman, *J. Phys. C, 19* (1986) 3877; M.F. Reid, *J. Chem. Phys., 87* (1987) 2875.
43 J.W. Lynn, in J.W. Lynn (ed.), *High Temperature Superconductivity*, Springer-Verlag, New York, 1990, p. 268 and refs. therein.
44 A. Furrer, P. Bruesch and P. Unternahrer, *Phys. Rev. B, 38* (1988) 4616.
45 K.W.H. Stevens, *Proc. Phys. Soc. A, 65* (1952) 209.
46 L. Soderholm, C.-K. Loong and S. Kern, *Phys. Rev. B, 45* (1992) 10062; *J. Alloys Comp., 181* (1992) 225.
47 L. Soderholm, W.-K. Kwok, G.L. Goodman and C.-K. Loong, *Eur. J. Solid State Chem., 28* (1991) 615.
48 L. Soderholm and C.-K. Loong, *J. Alloys Comp., 193* (1993) 125.
49 C.-K. Loong and L. Soderholm, in S.K. Malik and S.S. Shah (eds.), *High Temperature Superconductivity: Physical and Mechanical Properties*, Nova, New York, 1993, p. 257; C.-K. Loong and L. Soderholm, *Phys. Rev. B, 48* (1993) 14001.
50 L. Soderholm and C.-K. Loong, unpublished.
51 M.I. Bradbury and D.J. Newman, *Chem. Phys. Lett., 1* (1967) 45; D.J. Newman and G.E. Stedman, *J. Chem. Phys., 51* (1969) 3013; D.J. Newman and B. Ng, *Rep. Prog. Phys., 52* (1989) 699.
52 E.T. Heyen, R. Wegerer and M. Cardona, *Phys. Rev. Lett., 67* (1991) 144; E.T. Heyen, R. Wegerer, E. Schönberr and M. Cardona, *Phys. Rev. B, 44* (1991) 10195.
53 T. Ruf, E.T. Heyen, M. Cardona, J. Mesot and A. Furrer, *Phys. Rev. B, 46* (1992) 11792.
54 P. Allenspach, A. Furrer, P. Bruesch and P. Unternaehrer, *Physica B, 156–157* (1989) 864.